## Evidence of Rotational Fröhlich Coupling in Polaronic Trions

Maxim Trushin, <sup>1</sup> Soumya Sarkar, <sup>2</sup> Sinu Mathew<sup>†</sup>, <sup>2</sup> Sreetosh Goswami, <sup>2</sup> Prasana Sahoo, <sup>3</sup> Yan Wang, <sup>3</sup> Jieun Yang, <sup>3</sup> Weiwei Li, <sup>3</sup> Judith L. MacManus-Driscoll, <sup>3</sup> Manish Chhowalla, <sup>3</sup> Shaffique Adam<sup>\*</sup>, <sup>1,4,5</sup> and T. Venkatesan<sup>\*2,4,6</sup>

<sup>1</sup>Centre for Advanced 2D Materials, National University of Singapore, Singapore 117546

<sup>2</sup>NUSNNI NanoCore, National University of Singapore, Singapore 117411

<sup>3</sup>Department of Materials Science and Metallurgy,

University of Cambridge, Cambridge, UK CB30FS

<sup>4</sup>Department of Physics, National University of Singapore, Singapore, 117551

<sup>5</sup>Yale-NUS College, Singapore 138527

<sup>6</sup>Department of Electrical and Computer Engineering and Materials Science and Engineering,

National University of Singapore, Singapore 117583

(Dated: August 13, 2020)

Electrons commonly couple through Fröhlich interactions with longitudinal optical phonons to form polarons. However, trions possess a finite angular momentum and should therefore couple instead to rotational optical phonons. This creates a polaronic trion whose binding energy is determined by the crystallographic orientation of the lattice. Here, we demonstrate theoretically within the Fröhlich approach and experimentally by photoluminescence emission that the bare trion binding energy (20 meV) is significantly enhanced by the phonons at the interface between the two-dimensional semiconductor  $MoS_2$  and the bulk transition metal oxide  $SrTiO_3$ . The low-temperature binding energy changes from 60 meV in [001]-oriented substrates to 90 meV for [111] orientation, as a result of the counter-intuitive interplay between the rotational axis of the  $MoS_2$  trion and that of the  $SrTiO_3$  phonon mode.

Introduction — The quasiparticle concept is a powerful tool for understanding physics of many-body phenomena [1]. The concept was invented a few decades ago to describe the Fermi liquid [2], and later on applied to a broad range of phenomena including superconductivity [3, 4], magnetic ordering [5], and fractional quantum Hall effect [6]. The optically excited two-dimensional (2D) semiconductors contain tightly-bound excitons and trions — the quasiparticles composed of electrons and holes glued together by Coulomb forces [7]. Recently, yet another exhibit in this quasiparticle zoo — a polaronic trion was reported [8]. In this Letter, we demonstrate that a rotational optical (RO) phonon mode is necessary for the trion to engage in polaronic coupling that explains the underlying mechanism leading to formation of polaronic trions and enables significant tunability of trion binding energy (BE), a key to realize trion based optoelectronics.

In quasiparticle language, the conventional (Fröhlich [9, 10]) polaron is an electron dressed with phonons. The energy needed to undress the polaron (i.e. to release the electron) is the polaron BE. Typically, the strongest Fröhlich coupling occurs with longitudinal optical (LO) phonons in polar crystals with large difference between the static dielectric permittivity and its electronic contribution, such as in SrTiO<sub>3</sub> [11, 12]. However, the trionphonon interaction is distinct from coupling of phonons to free electrons. The outer electron in the trion is bound to the excitonic core (see Fig. 1), resulting in a finite angular momentum which enables stronger coupling with

RO rather than LO phonon modes. To maximize the effect, the trion's plane of rotation must match the polarization plane created by the RO mode (see Fig. 1). Hence, we can probe polaronic trions by either changing the Fröhlich coupling itself or the angle between rotational planes of the trion and the RO phonon mode. SrTiO<sub>3</sub> hosts RO phonons with very low vibration frequency [13] enabling an ideal environment to investigate the rotational Fröhlich coupling with trions. Notably, by changing the SrTiO<sub>3</sub> crystal orientation, one can tilt the rotational axis of the RO phonon mode and hence investigate the angular dependence of this coupling.

PL spectroscopy. — Monolayer MoS<sub>2</sub> is grown on single crystal SrTiO<sub>3</sub> substrates by chemical vapor deposition [14], and our samples are of comparable quality with those reported previously, see Supplemental Material [15] for sample characterization. We use three different crystallographic orientations of the SrTiO<sub>3</sub> substrate to tailor the polaronic effects in 2D MoS<sub>2</sub>. Fig. 2a shows the differential PL emission spectra of the excitonic (right) and trionic (left) peaks in the MoS<sub>2</sub> PL extracted from Lorentz fitting described in [15]. We have confirmed that the low energy peak is indeed a trion and does not arise from defect bound excitons through excitation power and electrostatic doping dependent measurements (Figs. S4) and S5 in [15]). The exciton-trion peak separation is the trion BE we are after. At low temperatures, the trionic peak splits further away from the excitonic peak position, and the splitting turns out to be dependent on the

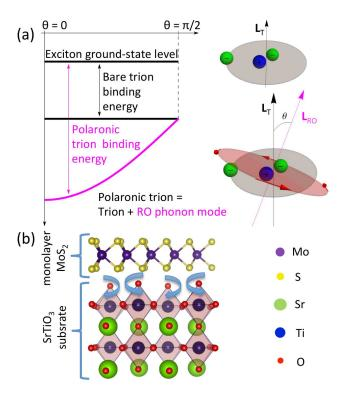


FIG. 1. (a) A trion consists of a tightly-bound excitonic core and an electron weakly coupled to the core by the electrondipole interactions. In a polaronic trion, a RO phonon mode couples with the tangential momentum of the outer electron increasing the resulting quasiparticle BE. The electrons and holes are represented by the green and blue balls, respectively. The tangential polarization generated by the RO phonon mode is shown by the red arrows. The black and magenta arrows show directions of the trion  $(\mathbf{L}_{\mathrm{T}})$  and RO phonon ( $\mathbf{L}_{\mathrm{RO}}$ ) angular momenta respectively, and  $\theta$  is the angle between them. The trion-phonon coupling maximizes at  $\theta = 0$  and vanishes at  $\theta = \pi/2$ , as shown by the polaronic trion BE curve (magenta). The bare trion BE does not depend on  $\theta$  at all. (b) Schematic of MoS<sub>2</sub>/SrTiO<sub>3</sub> heterostructure utilized to create rotational Fröhlich interactions. MoS<sub>2</sub> being an n-type semiconductor exhibits negatively charged trions. At low temperature, SrTiO<sub>3</sub> experiences structural cubic-to-tetragonal phase transition that activates the RO phonon mode due to the rotating TiO<sub>6</sub> octahedra (see also Fig. 3).

crystallographic orientation of the SrTiO<sub>3</sub> substrate. We have achieved BE enhancement of up to 60 meV that is enormous having in mind that bare trion BE is less than 30 meV. Fig. 2b shows the full width at half maximum (FWHM) for trionic and excitonic PL peaks. The trion FWHM experiences a significant broadening below the soft phonon activation temperature [13, 16]  $T_a \sim 132$  K, and the broadening turns out to be strongly dependent on the substrate orientation. In contrast, the exciton FWHM demonstrates much smaller broadening and weaker dependence on the substrate orientation. Finally, the exciton emission energy exhibits the usual monotonic

blue shift given by the Varshni relation [17] whereas the trion emission energy undergoes an unusual red shift below  $T_a$  (see Fig. 2c and Table S1 in [15]). The data presented in Fig. 2 all together indicates that the trion is not a conventional trion anymore but is an entirely new quasiparticle, the polaronic trion [8].

Trion Hamiltonian. — The trion can be seen as an electron weakly interacting with the excitonic core. The unperturbed Hamiltonian describing the relative electron-exciton motion can be written as

$$\hat{H}_0 = -\frac{\hbar^2}{2\mu_T} \left[ \frac{1}{r^2} \frac{\partial^2}{\partial \varphi^2} + \frac{1}{r} \frac{\partial}{\partial r} \left( r \frac{\partial}{\partial r} \right) \right]. \tag{1}$$

Here, we use polar coordinates  $\{\varphi,r\}$ . The trion reduced mass,  $\mu_T = m_X m_e/m_T$ , is defined in terms of the trion  $(m_T = m_X + m_e)$ , exciton  $(m_X = m_e + m_h)$ , electron  $(m_e)$ , and hole  $(m_h)$  effective masses, respectively. The energy in Eq. (1) is counted from the exciton ground-state level, as shown in Fig. 1a. The first (second) term in the square brackets is the tangential (radial) momentum operator with the eigenvalues  $k_{\varphi}$   $(k_r)$  given in units of the Planck constant  $\hbar$ . The electron-dipole interaction perturbing  $\hat{H}_0$  is much weaker than the direct Coulomb potential responsible for the exciton formation and rapidly vanishes at the distances much larger than the exciton size. This results in the trion BE much lower than that of exciton.

Rotational Fröhlich coupling. — The 2D Fourier transform of the polaronic interaction can be written as  $|V_q|^2 = 8\pi^2 e^2 F^2/q$ , where e is the elementary charge,  ${\bf q}$  is the in-plane wave vector, and F is a proportionality coefficient between the phonon mode amplitude and dielectric polarization created by this mode [18]. To express F in terms of macroscopic quantities we adopt an argument by Kittel [18] where the phonon perturbation producing dielectric polarization is equivalent to the Coulomb potential screened by the phononic part of the dielectric permittivity, i e

$$\frac{2e^2}{\hbar\omega} \sum_{\mathbf{Q}} \frac{(4\pi F)^2}{Q^2} e^{i\mathbf{Q}\cdot\mathbf{r}} = \left(\frac{1}{\epsilon_{\infty}} - \frac{1}{\epsilon_0}\right) \sum_{\mathbf{q}} \frac{2\pi e^2}{q} e^{i\mathbf{q}\cdot\mathbf{r}}, \quad (2)$$

where  $\epsilon_0$  ( $\epsilon_\infty$ ) is the static (high-frequency) dielectric permittivity at the MoS<sub>2</sub>/SrTiO<sub>3</sub> interface,  $\hbar\omega$  is the phonon energy quantum,  ${\bf r}$  is the in-plane coordinate,  ${\bf Q}$  is the phonon wave vector whose absolute value can be written in terms of in-plane (q) and axial ( $q_{\parallel}$ ) components as  $Q=\sqrt{q_{\parallel}^2+q^2-2qq_{\parallel}\cos(\pi/2+\theta)}$ . The axial component does not contribute to rotational Fröhlich coupling and can be integrated out easily. The resulting polarization turns out to be  $\theta$  dependent,  $F=\sqrt{\hbar\omega\cos\theta\left(\epsilon_{\infty}^{-1}-\epsilon_{0}^{-1}\right)/(8\pi)}$ , and the 2D Fourier transform of the polaronic potential reads

$$V_q = -i\hbar\omega\sqrt{\cos\theta}\sqrt{\frac{2\pi\alpha r_\omega}{q}},\tag{3}$$

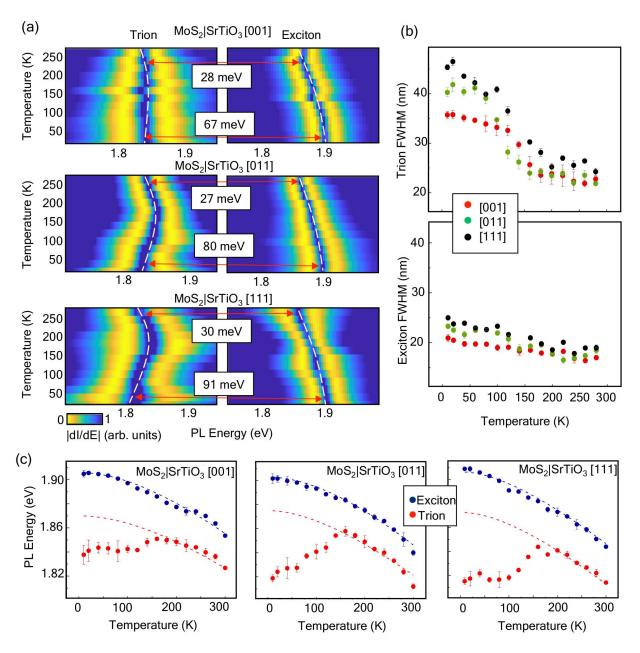


FIG. 2. (a) Pseudocolor map of the differential PL emission intensity (|dI/dE|) from 2D MoS<sub>2</sub> demonstrates two quasiparticle peaks attributed to excitons and trions. The splitting between them depends on temperature and SrTiO<sub>3</sub> substrate orientation with the strongest separation for [111]-oriented SrTiO<sub>3</sub> crystals below 50 K. (b) Temperature dependence of FWHM for trionic (upper panel) and excitonic (lower panel) PL quasiparticle peaks for different SrTiO<sub>3</sub> substrate orientations indicates much stronger Fröhlich interactions for the former than for the latter. (c) Extracted trionic and excitonic PL energies vs. temperature with the corresponding Varshni fits as dashed lines indicate anomalous behavior of the PL trion peak below 132 K. The error bars are standard error for three samples.

where  $r_{\omega} = \sqrt{\hbar/2\mu_T\omega}$  is the interaction length, and

$$\alpha = \frac{e^2}{2\hbar\omega r_\omega} \left( \frac{1}{\epsilon_\infty} - \frac{1}{\epsilon_0} \right) \tag{4}$$

is the standard Fröhlich coupling constant [9]. The striking difference between the standard 2D polaronic interaction [11, 18] and Eq. (3) is the  $\sqrt{\cos \theta}$  pre-factor that occurs due to the special direction singled out by the an-

gular momentum of a RO phonon mode. Note that the effective mass in  $r_{\omega}$  is given by  $\mu_T$  instead of  $m_e$  as in the conventional case [11].

Polaronic perturbation. — In the non-perturbed limit, when both dipole and polaronic perturbations vanish, the plane-wave solution suggests the kinetic energy  $E_{\bf k}$  of the relative electron-exciton motion be a sum the radial  $\hbar^2 k_r^2/2\mu_T$  and tangential  $\hbar^2 k_\varphi^2/2\mu_T$  terms. The latter

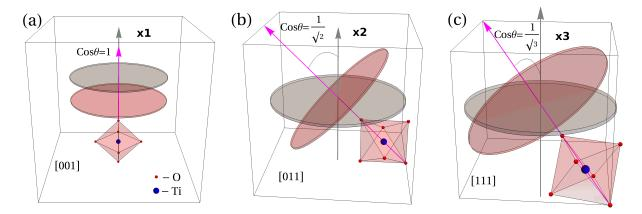


FIG. 3. (a) In a [001]-oriented SrTiO<sub>3</sub> domain, the TiO<sub>6</sub> octahedra rotate in the same plane as the trion in 2D MoS<sub>2</sub> placed on top. Here, the trion's and RO phonon planes of rotation are shown by the gray and reddish discs, respectively. (b,c) Once the SrTiO<sub>3</sub> substrate orientation changes, the rotational axes of the trion and RO phonon mode (depicted by black and magenta arrows, respectively) do not align anymore and span the angle  $\theta$  determined by the domain orientation. The bold numbers indicate the number of mutually perpendicular domain orientations contributing to the polaronic trion BE.

is quantized in any circularly symmetric potential, however, we assume that the normalization length is long enough to justify integration instead of summation and map tangential and radial momenta onto the Cartesian coordinates. We note that within the Fröhlich approach, the angular momenta indicated in Fig. 1 are quasiclassical quantities and not associated with the s or p quantum states. The perturbation theory suggests the following expression for the polaronic energy correction [18]

$$E_P = -\int \frac{d^2q}{(2\pi)^2} \frac{|V_q|^2}{E_{\mathbf{k}} - E_{\mathbf{k}-\mathbf{q}} - \hbar\omega}.$$
 (5)

We evaluate Eq. (5) for the BE correction  $(\mathbf{k} \to 0)$ . Despite the electron-exciton relative motion being 2D, the rotational polaronic coupling is effectively 1D. This is because RO phonon modes produce no radial polarization (hence, no radial electric field, see Fig. 1a), and, therefore, the energy difference  $E_{\mathbf{k}} - E_{\mathbf{k}-\mathbf{q}}$  does not contain  $q_r$ . The BE correction can then be written as

$$E_P = \frac{2}{\pi} \int_0^\infty dq_r \int_0^\infty dq_\varphi \frac{\hbar^2 \omega^2 \alpha r_\omega \cos \theta}{\sqrt{q_\varphi^2 + q_r^2}} \frac{2\mu_T/\hbar^2}{q_\varphi^2 + r_\omega^{-2}}$$
$$= \alpha \hbar \omega \cos \theta \ln (2r_\omega/a), \qquad (6)$$

where 1/a is a momentum cut-off. Similar to the conventional expression for the 2D polaron BE,  $E_P = \frac{\pi}{2} \alpha \hbar \omega$ , our result is linear in  $\alpha$  (this also holds beyond perturbation theory, see e.g. Refs. [11, 19, 20]) and linear in phonon energy  $\hbar \omega$ , setting the scale of polaronic interactions. However, Eq. (6) is different in two important ways: since the RO phonon modes are decoupled from both the axial and radial electron motion, this results respectively in the  $\cos \theta$  and  $\ln (2r_{\omega}/a)$  pre-factors (the latter is a weak function of the order of unity and less important than the former). The logarithmic divergence

is a well-known property of the Fröhlich coupling in a 1D limit [21]. The length a is the lattice constant that determines the first Brillouin zone size in MoS<sub>2</sub>. If  $q_r$  is retained in the denominator of Eq. (5), and  $\theta$  is set to zero, we recover the conventional result.

Discussion. — The dressed trion BE is  $E_{PT} = E_P +$  $E_T$ , where  $E_T$  is the bare trion binding energy. To make predictions regarding BE in realistic samples the multidomain structure of the SrTiO<sub>3</sub> substrate must be taken into account. The axis of antiphase rotation of neighboring oxygen TiO<sub>6</sub> octahedra is different in each domain [22]. We assume that the domain orientation is perfectly random, so that any of three mutually perpendicular orientations are weighted equally in the BE calculation. In the simplest case of the [001]-grown substrate, the rotational axis of RO mode in [001]-oriented domain is normal to the trion plane and the polaronic effect is maximal (see Fig. 3a). The other two [010]- and [100]-oriented domains do not contribute at all because the phonon mode rotation axis is parallel to the trion plane and  $\theta = \pi/2$ in Eq. (6). Hence, the total  $E_{PT}$  reads

$$E_{PT}[001] = E_T + \alpha \hbar \omega \ln (2r_{\omega}/a). \tag{7}$$

In the case of either [011] or [101] domain orientation we have  $\cos \theta = 1/\sqrt{2}$  (see Fig. 3b). The [110]-oriented domains do not contribute here, and  $E_{PT}$  reads

$$E_{PT}[011] = E_T + \sqrt{2}\alpha\hbar\omega \ln(2r_\omega/a). \tag{8}$$

The [111] orientation suggests  $\cos \theta = 1/\sqrt{3}$  (see Fig. 3c), and all three possible mutually perpendicular domain orientations do contribute equally. Hence, we have

$$E_{PT}[111] = E_T + \sqrt{3}\alpha\hbar\omega \ln\left(2r_\omega/a\right). \tag{9}$$

The BE is shown in Fig. 4 as a function of temperature for different substrate orientations. The highest BE

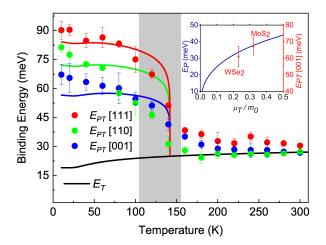


FIG. 4. Temperature dependence of the polaronic trion BE measured for three different substrate orientations along with  $E_{PT}$  given by Eqs. (7,8,9), respectively. The shaded transition region corresponds to  $T_c^{\rm bulk} < T < T_c^{\rm surface}$  with  $T_c^{\rm bulk}$  and  $T_c^{\rm surface}$  being the bulk and surface structural transition temperatures, respectively [23]. The model is not expected to fit BE in that region. The bare trion energy [24]  $(E_T)$  is shown for comparison. The error bars are standard error for three samples. Inset: Polaronic trion BE measured at 10 K for MoS<sub>2</sub> and WSe<sub>2</sub> on the same [001]-oriented SrTiO<sub>3</sub> substrate (right axis) follows the theoretical trend predicted by Eq. (6) at T=0 (left axis). We avoid plotting theoretical  $E_{PT}$ , as we do not know the phenomenological  $E_T$  for WSe<sub>2</sub>.

 $(\sim 90~{\rm meV})$  is achieved for [111]-grown substrate despite the smallest  $\cos\theta=1/\sqrt{3}$  (hence, the weakest coupling) for [111]-domain orientation. This is almost twice larger than the highest trion BE reported so far in n-doped  ${\rm MoS}_2$  ( $\sim 40~{\rm meV}$  [24],  $\sim 50~{\rm meV}$  [25]). Moreover, the polaronic trion BE allows for 200% tunability (from  $\sim 30~{\rm meV}$  to  $\sim 90~{\rm meV}$ ), which far exceeds that possible by conventional electrostatic gating [25]. The bare trion energy  $E_T$  (black line) is estimated using the phenomenological approach of Ref. [24]. Eqs. (7,8,9) combined with the material parameters,  $\epsilon_0(T), \epsilon_\infty$ , and  $\omega(T)$ , are able to explain the measured polaronic trion BE behaviour for all crystallographic orientations of the substrate. We do not adjust the material parameters, see Supplemental Material [15], which also includes Refs. [13, 14, 16, 17, 23–40].

The polaronic effect we have discovered is not limited to trions in MoS<sub>2</sub>. We have tested a few similar samples where MoS<sub>2</sub> has been substituted by WSe<sub>2</sub> and found the same PL features as shown in Fig. 2. The PL emission from WSe<sub>2</sub>/SrTiO<sub>3</sub> at 10 K (see Fig. S7 in [15]) shows spectral broadening and an anomalous enhancement in the energy separation between the exciton and trion peak (as compared with the spectra at 300 K), suggesting an increased trion binding energy. The polaronic trion BE in WSe<sub>2</sub> has turned out to be a little lower than in MoS<sub>2</sub>, see inset in Fig. 4 for comparison. As

the high-frequency dielectric permittivity is the same for both  $\mathrm{MoS}_2$  and  $\mathrm{WSe}_2$  [29], we attribute this difference to the lower effective mass in  $\mathrm{WSe}_2$  [31, 33], see [15] for details.

Outlook. — The polaronic trion discussed here is a complex three-component quasiparticle comprising the exciton core, an electron, and an RO phonon mode coupled together by both Coulomb and Fröhlich interactions, resulting in a large enhancement of the BE. Since the polaronic interaction length  $r_{\omega}$  is much larger than the lattice constant, we expect these polaronic trions to only weakly depend on SrTiO<sub>3</sub> surface termination [41]. Despite its complexity we have shown that the quasiparticle can live in 2D semiconductors other than MoS<sub>2</sub>. We therefore anticipate further discoveries revealing a hierarchy of energy-rich quasiparticles [42] optically excited in 2D semiconductors with unconventional substrates underneath.

Acknowledgements. — M.T. is supported by the Director's Senior Research Fellowship at CA2DM (Singapore NRF Medium-Sized Centre Programme R-723-000-001-281, NUS Young Investigator Award R-607-000-236-133). S.S., S.G., and T.V. acknowledge support from the National Research Foundation, Singapore under Competitive Research Program (NRF2015NRF-CRP001-015). S.M. acknowledges support from NUSNNI general purpose account grant IN-398-000-006-001 and international atomic energy agency (IAEA) CRP (F11020).

Author contributions. — M.T. and S.S contributed equally. M.T. devised the model. S.S. grew the  $\mathrm{MoS}_2$  samples on  $\mathrm{SrTiO}_3$  with the help of S.M. and performed the PL spectroscopy. P.S., Y.W., J.Y., W.L., J.L.M. and M.C. provided the  $\mathrm{WSe}_2/\mathrm{SrTiO}_3$  samples. All the authors discussed and analysed the data. T.V. and S.A. supervised the project.

\* corresponding authors.

 $^\dagger$ present address: Department of Physics, S. B. College, Mahatma Gandhi University, Kerala 686101 India.

L. Venema, B. Verberck, I. Georgescu, G. Prando,
 E. Couderc, S. Milana, M. Maragkou, L. Persechini,
 G. Pacchioni, and L. Fleet, Nature Physics 12, 1085 (2016).

<sup>[2]</sup> L. D. Landau, Sov. Phys. JETP 3, 920 (1956).

<sup>[3]</sup> N. N. Bogoljubov, Il Nuovo Cimento (1955-1965) 7, 794 (1958)

<sup>[4]</sup> J. G. Valatin, Il Nuovo Cimento (1955-1965) 7, 843 (1958).

<sup>[5]</sup> A. V. Chumak, V. I. Vasyuchka, A. A. Serga, and B. Hillebrands, Nature Physics 11, 453 (2015).

<sup>[6]</sup> R. B. Laughlin, Rev. Mod. Phys. **71**, 863 (1999).

<sup>[7]</sup> K. F. Mak and J. Shan, Nature Photonics 10, 216 (2016).

<sup>[8]</sup> S. Sarkar, S. Goswami, M. Trushin, S. Saha, M. Panahandeh-Fard, S. Prakash, S. J. R. Tan, M. Scott, K. P. Loh, S. Adam, S. Mathew, and T. Venkatesan, Advanced Materials 31, 1903569 (2019).

<sup>[9]</sup> H. Fröhlich, Advances in Physics 3, 325 (1954).

- [10] R. P. Feynman, Phys. Rev. 97, 660 (1955).
- [11] J. T. Devreese, Encycl. Appl. Phys. 14, 383 (1996).
- [12] H. Takashima, R. Wang, B. Prijamboedi, A. Shoji, and M. Itoh, Ferroelectrics 335, 45 (2006).
- [13] J. Petzelt, T. Ostapchuk, I. Gregora, I. Rychetský, S. Hoffmann-Eifert, A. V. Pronin, Y. Yuzyuk, B. P. Gorshunov, S. Kamba, V. Bovtun, J. Pokorný, M. Savinov, V. Porokhonskyy, D. Rafaja, P. Vaněk, A. Almeida, M. R. Chaves, A. A. Volkov, M. Dressel, and R. Waser, Phys. Rev. B 64, 184111 (2001).
- [14] A. M. Van Der Zande, P. Y. Huang, D. A. Chenet, T. C. Berkelbach, Y. You, G.-H. Lee, T. F. Heinz, D. R. Reichman, D. A. Muller, and J. C. Hone, Nature Materials 12, 554 (2013).
- [15] Supplemental Material can be found below.
- [16] P. A. Fleury, J. F. Scott, and J. M. Worlock, Phys. Rev. Lett. 21, 16 (1968).
- [17] Y. Varshni, Physica 34, 149 (1967).
- [18] C. Kittel, Quantum theory of solids (Wiley, New York, 1987).
- [19] S. Das Sarma and B. A. Mason, Annals of Physics 163, 78 (1985).
- [20] W. Xiaoguang, F. M. Peeters, and J. T. Devreese, Phys. Rev. B 31, 3420 (1985).
- [21] F. M. Peeters and M. A. Smondyrev, Phys. Rev. B 43, 4920 (1991).
- [22] Y.-Y. Pai, A. Tylan-Tyler, P. Irvin, and J. Levy, Reports on Progress in Physics 81, 036503 (2018).
- [23] Z. Salman, M. Smadella, W. A. MacFarlane, B. D. Patterson, P. R. Willmott, K. H. Chow, M. D. Hossain, H. Saadaoui, D. Wang, and R. F. Kiefl, Phys. Rev. B 83, 224112 (2011).
- [24] Y. Lin, X. Ling, L. Yu, S. Huang, A. L. Hsu, Y.-H. Lee, J. Kong, M. S. Dresselhaus, and T. Palacios, Nano Letters 14, 5569 (2014).
- [25] K. F. Mak, K. He, C. Lee, G. H. Lee, J. Hone, T. F. Heinz, and J. Shan, Nature Materials 12, 207 (2013).
- [26] D. K. Efimkin and A. H. MacDonald, Phys. Rev. B 95, 035417 (2017).
- [27] E. Sawaguchi, A. Kikuchi, and Y. Kodera, Journal of the Physical Society of Japan 17, 1666 (1962)
- [28] J. H. Barrett, Phys. Rev. 86, 118 (1952).
- [29] A. Laturia, M. L. Van de Put, and W. G. Vandenberghe, npj 2D Materials and Applications 2, 6 (2018).
- [30] C. Lasota, C.-Z. Wang, R. Yu, and H. Krakauer, Ferroelectrics 194, 109 (1997).
- [31] T. C. Berkelbach, M. S. Hybertsen, and D. R. Reichman, Phys. Rev. B 88, 045318 (2013).
- [32] N. Lu, H. Guo, L. Wang, X. Wu, and X. C. Zeng, Nanoscale 6, 4566 (2014).
- [33] M. Luisier, A. Szabo, C. Stieger, C. Klinkert, S. Brück, A. Jain, and L. Novotny, in 2016 IEEE International Electron Devices Meeting (IEDM) (2016) pp. 5.4.1–5.4.4.
- [34] N. Wakabayashi, H. G. Smith, and R. M. Nicklow, Phys. Rev. B 12, 659 (1975).
- [35] C. Lee, H. Yan, L. E. Brus, T. F. Heinz, J. Hone, and S. Ryu, ACS Nano 4, 2695 (2010).
- [36] S. Tongay, J. Suh, C. Ataca, W. Fan, A. Luce, J. S. Kang, J. Liu, C. Ko, R. Raghunathanan, J. Zhou, et al., Scientific Reports 3, 2657 (2013).
- [37] W. Zhao, Z. Ghorannevis, K. K. Amara, J. R. Pang, M. Toh, X. Zhang, C. Kloc, P. H. Tan, and G. Eda, Nanoscale 5, 9677 (2013).
- [38] K. He, N. Kumar, L. Zhao, Z. Wang, K. F. Mak, H. Zhao,

- and J. Shan, Phys. Rev. Lett. 113, 026803 (2014).
- [39] V. Chellappan, A. L. C. Pang, S. Sarkar, Z. E. Ooi, and K. E. J. Goh, Electronic Materials Letters 14, 766 (2018).
- [40] A. M. Jones, H. Yu, N. J. Ghimire, S. Wu, G. Aivazian, J. S. Ross, B. Zhao, J. Yan, D. G. Mandrus, D. Xiao, et al., Nature Nanotechnology 8, 634 (2013).
- [41] A. Schrott, J. Misewich, M. Copel, D. Abraham, and Y. Zhang, Applied Physics Letters 79, 1786 (2001).
- [42] M. Barbone, A. R.-P. Montblanch, D. M. Kara, C. Palacios-Berraquero, A. R. Cadore, D. De Fazio, B. Pingault, E. Mostaani, H. Li, B. Chen, et al., Nature Comm. 9, 3721 (2018).

## Supplemental Material

Sample Growth — The growth of  $MoS_2$  was carried out using 4 inch quartz tube inside a single-zone tube furnace (Thermcraft). Sulfur powder (Sigma-Aldrich, 99.99% pure) was kept outside the hot zone and  $MoO_3$  powder (Sigma-Aldrich, 99.999% pure) and high purity STO substrates of different crystal orientations (CrysTec GmbH) were placed at the center of the hot-zone. Atmospheric pressure CVD growth is performed using high purity nitrogen gas as the carrier gas. The growth temperature was at  $700^{\circ}$  C, and we followed the method by van der Zande et al. [14].

Optical Spectroscopy Methods — The Raman and PL spectroscopy were carried out using JY Horiba LabRAM HR Evolution Raman Spectrometer in the backscattering geometry. The excitation radiation was 514.5 nm from a Lexel SHG 95 Argon ion laser. To avoid any thermal effects, the power of the laser incident on our sample was less than 500  $\mu$ W for the above measurements. A long working distance 50X objective was used for the above measurements and the spot size of the laser beam was focused to 1-2  $\mu$ m. A helium closed cycle refrigerator cooled cryogenic stage with optically transparent window were used to collect PL spectra from 300 K to 10 K. A computer controlled motorized XY stage was used in order to record the PL mapping of the sample under study.

Polaronic trion binding energy fitting — The bare trion binding energy can be estimated perturbatively [26], but we assume the phenomenological formula [24]  $E_T(\epsilon_0) = E_T(1)/\epsilon_0^{\beta_T}$ , where  $\beta_T = 0.085$  is a constant,  $E_T(1) = 42$  meV is  $E_T$  at  $\epsilon_0 = 1$ . The polaronic contribution is calculated using the theory introduced in the main text and material constants discussed below.

Static dielectric screening on the  $MoS_2/STO$  interface is largely dominated by STO, especially at low temperatures, when the relative dielectric permittivity exceeds  $10^4$  [27]. This is governed by the Curie-Weiss law modified by Barrett [28], and we set accordingly

$$\epsilon_0 = \frac{T_2}{\frac{T_1}{2} \coth\left(\frac{T_1}{2T}\right) - T_C},$$

where  $T_2 = 9 \cdot 10^4$  K,  $T_1 = 84$  K, and Curie temperature  $T_C = 38$  K. In contrast, the high-frequency screen-

ing is dominated by the 2D semiconductor [29] with the in-plane dielectric permittivity  $\epsilon_{\infty}=15.1$ , substantially higher than that for STO [30]. The RO phonon frequency is dominated by the  $A_{1g}$  mode with the temperature dependence given by [13, 16]  $\omega=\omega_0\left(1-T/T_a\right)^{\frac{1}{3}}$ , where  $T\leq T_a$ ,  $\hbar\omega_0=7$  meV, and the mode activation temperature is  $T_a=132$  K.

We emphasize that our activation temperature  $T_a=132~{\rm K}$  is different from the STO phase transition temperature around 105 K. This is because the interfacial nature of the effect considered. The trions excited in 2D MoS<sub>2</sub> interact with the rotational phonons located on or very near to the STO surface, not with the bulk ones. As it is shown in Ref. [23], the phase transition starts in the near-surface regions at temperatures much higher than the bulk transition temperature of about 105 K. In fact, it can be as high as 155 K for some surface domains. The higher surface transition temperature is probably responsible for the higher activation temperature of the rotational  $A_{1g}$  phonon mode found by means of Raman spectroscopy [13].

The difference between the surface and bulk critical temperatures can be seen in our measurements: The trionic binding energy stops decreasing with temperature near 150 K, but the trend is not obvious until the temperature drops below 135 K. At T < 105 K the transition is complete, and the temperature dependence of the binding energy is determined by that of the soft phonon frequency and static dielectric constant. Our model does not distinguish the domains by their preferred transition temperature, and this is the reason why the theoretical binding energy is such a sharp function of T. We could try to modify the theory to account for different domains switching at different temperatures giving some broadening; however, we choose instead to keep the theory without any fitting parameters.

The remaining material constants for MoS<sub>2</sub> represent effective masses  $m_e = 0.46m_0$ ,  $m_h = 0.56m_0$  [31–33] ( $m_0$  is the free electron mass), and the lattice constant  $a = 3.15 \,\text{Å}$  [34]. As far as WSe<sub>2</sub> is concerned, the high-frequency dielectric permittivity remains the same as for MoS<sub>2</sub> [29], but the effective masses are somewhat lower, namely,  $m_e = 0.33m_0$ ,  $m_h = 0.43m_0$  [31, 33].

Since there are no adjustable parameters, the minor quantitative disagreement should not take away from our main conclusion about the dependence of binding energy on substrate orientation, for which the theory and experiment are well matched.

#### Section S1: Sample Characterization

See Figures S1 and S2.

#### Section S2: Lorentz Fitting of PL Spectra

Fitting Principle — We have used the standard curve fitting software to fit our  $MoS_2$  PL spectra. As the

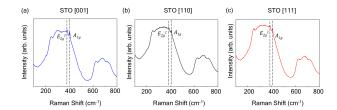
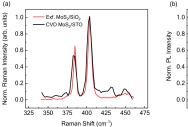


FIG. **S1**. Raman spectra of monolayer MoS<sub>2</sub> grown on (a) STO [001] (b) STO [110] and (c) STO [111]. The black dashed lines indicate the characteristic Raman modes for 2H-MoS<sub>2</sub> with the strong second order vibrational modes of STO [13] in the background. The separation between the in-plane (E<sub>2g</sub>) and out-of-plane (A<sub>1g</sub>) vibrational modes of MoS<sub>2</sub> is  $\sim 20$  cm<sup>-1</sup>, which indicates that our sample is a monolayer [35].



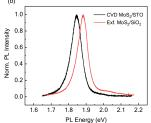


FIG. S2. Comparison of (a) Raman and (b) PL spectra of an exfoliated monolayer  $MoS_2$  (in our lab) with  $MoS_2/STO$ . In the Raman spectra, both the characteristic in-plane  $E_{2g}$  and out-of-plane  $A_{1g}$  modes in  $MoS_2/STO$  (after background correction of STO Raman spectra) and  $MoS_2/SiO_2$  show a similar linewidth and intensity ratio that suggests that the sample is of good quality and there is no substrate induced charge doping in  $MoS_2/STO$ . The PL spectra too shows identical spectral shape and linewidth. The PL peak in  $MoS_2/STO$  is redshifted as compared to the PL emission on  $MoS_2/SiO_2$  due to dielectric screening [24] from the substrate.

PL of  $MoS_2$  cannot be fitted using a single Lorentzian curve due to spectral asymmetry we use 3 Lorentzian curves (standard practice in the community) corresponding to the A exciton,  $A^-$  trion, and B exciton. The Lorentzian curves are initialized and then allowed to adjust through multiple iterations to obtain the best cumulative fit that closely matches the experimental raw data. For all our fits, the coefficient of determination in the regression model COD (R2)  $\sim 0.99$  providing a satisfactory fit, as shown in Figure S3.

**Determination of Peak Position** — The peak position of each individual quasiparticle has been determined from the peak center of their corresponding Lorentz spectrum.

**Determination of Peak Width** — The linewidth of each individual quasiparticle has been determined from the FWHM of their corresponding Lorentz spectrum.

**Table S1** — Varshni fit [17],  $E = E_0 - AT^2/(T+B)$ , parameters for the A exciton (upper) and A<sup>-</sup> trion

(lower) energy in  $\mathrm{MoS}_2$  grown on different substrate orientations.

Sample	$E_0$ (eV)	$A (eV/K^2)$	B(K)
$MoS_2/STO$ [001]		$4.55 \cdot 10^{-4}$	480
$MoS_2/STO$ [011]	1.902	$5.45 \cdot 10^{-4}$	569
$MoS_2/STO$ [111]	1.906	$4.1 \cdot 10^{-4}$	310
$MoS_2/STO$ [001]	1.868	$2.55 \cdot 10^{-4}$	482
$MoS_2/STO$ [011]	1.875	$3.93 \cdot 10^{-4}$	360
$MoS_2/STO$ [111]	1.873	$4.2\cdot 10^{-4}$	307

Section S3: Excitation Power Dependent PL Spectra

See Figure S4 below.

### Section S4: Identification of Trions by Electrostatic Gating

We have performed electrostatic gate dependent measurement of the PL intensity to confirm the identity of

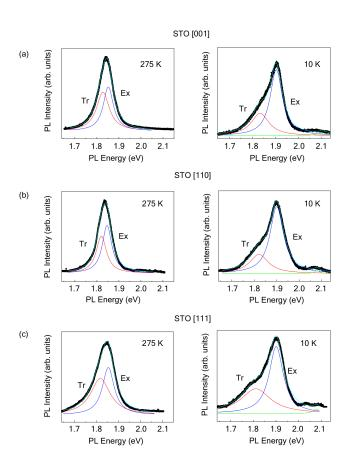


FIG. S3. PL spectra at 275 K (left) and 10 K (right) fitted with 3 different Lorentzian peaks for  $MoS_2$  on (a) STO [001] (b) STO [110] and (c) STO [111]. The cumulative curve fit shows a close match with the experimental data. Red curve:  $A^-$  trion; blue curve: A exciton; green curve: B exciton; cyan curve: cumulative fit.

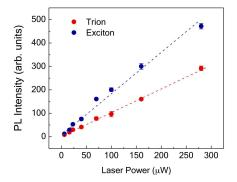


FIG. **S4**. PL intensity of the exciton and trion in MoS<sub>2</sub>/STO [001] as a function of incident laser excitation power at 10 K. Both the exciton and trion peaks have a linear power dependence, as it has been reported previously, in contrast to the defect emission, which is expected to saturate at higher powers when the defects are fully populated with excitons [36].

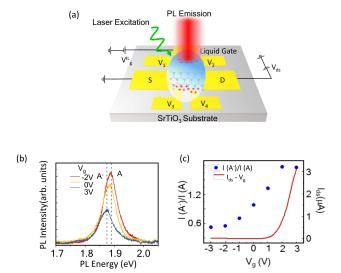


FIG. S5. (a) Schematics of our device for measuring PL emission as a function of electrostatic gate voltage. (b) PL spectra as a function of top gate voltage. (c) Intensity ratio of the trion to exciton component (blue dots) of the PL spectra as a function of top gate voltage correlated with the  $I_{ds}$ – $V_g$  characteristics (red curve).

the quasiparticles. As shown in Figure S5(c), when we move towards the electron rich n-regime (evident from the  $I_{ds}$ - $V_g$  characteristics), the intensity ratio of the trion to exciton peaks in the PL spectra increases, a phenomena generally associated to the spectral weight transfer from the neutral exciton to the charged trion [25]. This provides definitive evidence of the charge nature of the peaks and confirms that the measured spectra are due to trions rather than defects.

# Section S5: Investigating WSe<sub>2</sub>/STO

See Figures **S6** and **S7**.

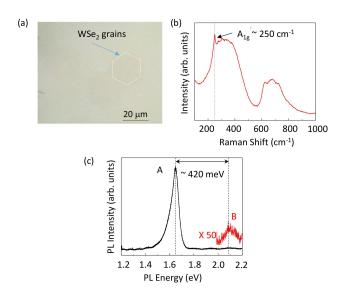


FIG. S6. (a) Optical image of WSe<sub>2</sub>/STO. The white hexagon is a guide to the eye to help locate the WSe<sub>2</sub> crystals that have poor optical contrast due to the transparent STO substrate. (b) Raman spectra of WSe<sub>2</sub>/STO. The characteristic  $A_{1g}$  mode [37] is observed at  $\sim 250~\rm cm^{-1}$  with a wide background that is associated with the STO Raman spectra. (c) PL spectra of monolayer WSe<sub>2</sub>/STO shows a direct bandgap emission at 1.65 eV and a weak B exciton  $\sim 2.1~\rm eV$  consistent with previous reports from high quality samples [38, 39].

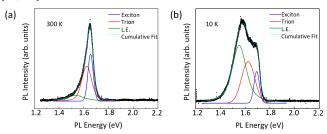


FIG. S7. PL Spectra of WSe<sub>2</sub>/STO at (a) 300 K and (b) 10 K fitted with three peaks (consistent with previous reports) that represent the neutral exciton (blue), charged trion (red), and localized exciton (L.E.). The cyan curve is the cumulative fit. One can observe spectral broadening and enhancement of the separation of the excitonic and trionic emission energies, that translates to a higher trion binding energy (TBE). This is in clear contrast to several reports [39, 40] on WSe<sub>2</sub>/SiO<sub>2</sub> that show sharp excitonic resonances and absence of TBE enhancement of low temperature, suggesting polaronic phenomena at the WSe<sub>2</sub>/STO interface.